

Phase diagram for a single flexible magnetic filament in a poor solvent at zero field

Joan J. Cerdà,^{*a‡} Pedro A. Sánchez,^b Christian Holm,^b and Tomàs Sintes^a

The equilibrium conformations of a flexible permanent magnetic chain that consists of a sequence of linked magnetic colloidal nanoparticles with short-ranged attractive interactions are thoroughly analysed via Langevin dynamics simulations. A tentative phase diagram is presented in the limit of infinite dilution. We find that the phase diagram of such colloidal polymers exhibits several unusual conformational phases when compared with the non-magnetic chains. These are characterised by a large degree of conformational anisotropy: simple closed chains, helicoidal-like states, partially collapsed states, and very compact disordered states. The phase diagram shows several interesting features like the existence of at least two 'triple points'.

1 Introduction

Artificial magnetic filaments can be obtained by mutually linking magnetic colloids to form a chain. These magnetic chains represent the equivalent to magnetic polymers but at supra-molecular scale. Magnetic polymers have magnetic properties only at $T < 100\text{K}$ ^{1,2}, magnetic filaments can retain their magnetism at zero field and room temperature if the size of the nanocolloids is chosen adequately. Although the exact range may depend strongly on the type of materials used, common magnetic cores with sizes between 10 and 100nm can exhibit a permanent dipolar moment if they are single magnetic domains blocked in the crystal lattice of the particle³. Cores smaller than 10nm are expected to exhibit a superparamagnetic behaviour due to the dominance of Néel relaxation processes. Cores larger than 100nm are expected to show paramagnetic properties due to the formation of multiple magnetic domains⁴.

The path towards the synthesis of such permanent magnetic filaments has been possible thanks to a progressive increase in the abilities to control the size of magnetic colloids and the nature of bonds between the colloidal particles⁵. Initially, Furst et al.^{6,7} reported in their seminal papers the use of micron-sized magnetic-filled paramagnetic latex beads as monomers to form magnetic chains. Further progress was achieved by Dreyfus et al.⁸ using DNA to link micron-sized paramagnetic beads. The first steps towards the assembly of magnetic filaments using sub-micrometric particles (0.5 – 0.8 μm) where reported by Tabata et al.⁹ Magnetic chains with lengths in the range 30 to 50 μm , either in solution or attached to a surface, were presented by Singh et al.^{10,11} and Toonder et al.¹² Shorter magnetic chains synthesised using sub-micrometric colloids in an electrolyte solution^{13,14} and via single-step syn-

thesis¹⁵ have also been achieved. On the other hand, the synthesis of arrays made of long magnetic filaments (from 1 to 200 μm) with length-to-monomer-size ratios up to 125 times were obtained by Evans and co-workers¹⁶.

Further technological improvements allowed the use of nanoparticles with sizes below 50nm that form mesoscopic one-dimensional structures^{17–23}. Very recently, Benkoski et al.^{24,25} have reported the optical visualisation of small ferromagnetic cobalt nanoparticles (23.5nm) organised into microscopic one-dimensional chains without needing to resort to templates or multiple fabrication steps. Those filaments can be attached to a surface and form brush-like structures by conveniently arranging some magnets along the surface^{24,26}. Very recently, Sarkar and Mandal²⁷ have performed a noteworthy synthesis of magnetic chains using DNA as a template on which they directly grow the magnetic nanoparticles with sizes ranging between 7 and 17 nanometers. The particles remain anchored to the DNA, and the whole system behaves as a magnetic filament. It is also worthwhile to point out that there have been successful attempts by Zhou et al. to lock and preserve the structural conformations of filaments made of magnetic cobalt nanocolloids of 20nm in size¹⁷. Goubault²⁸ et al. have achieved the synthesis of flexible magnetic filaments by the simple procedure of bridging the surfactant layers that ferrofluid particles carry adsorbed on top of their surface in presence of an external magnetic field. Once the bridging has occurred, the filaments are irreversibly formed and the external magnetic field can be removed.

The emerging interest in this relatively novel field is due to the fact that magnetic filaments are very appealing from the technological point of view. They can be thought as improved substitutes of current ferrofluids, or as elements for magnetic memories, chemical and pressure nanosensors, or medical applications, to mention just a few⁵. Furthermore, the study of the structures adopted by magnetic filaments is also of relevance in the area of inverse ferrofluids where non-magnetic particles are added to a ferrofluid solution. Those particles will behave inside the ferrofluid equivalently to that

^a Instituto de Física Interdisciplinar y Sistemas Complejos, IFISC (CSIC-UIB), Universitat de les Illes Balears. E-07122 Palma de Mallorca, Spain.

^b Institute for Computational Physics, Universität Stuttgart. 70569 Stuttgart, Germany.

‡ E-mail: joan@ifisc.uib-csic.es

an ordinary magnetic particle would do in a non-magnetic solvent²⁹. By linking a sequence of non-magnetic nanocolloids to form chains and immersing them in a ferrofluid, we can have exactly the same behaviour for those colloidal chains as for true magnetic filaments in an ordinary non-magnetic solvent. The use of such 'polymer colloids' in ferrofluids can have also many potential applications. For instance, 'inverse filaments' have already been used in the assembly of photonic crystals that only exist during the time that an external magnetic field is applied to the sample³⁰. In general, in most of the applications, the knowledge of the different types of equilibrium structures that filaments may adopt can be of extreme importance. Nonetheless, so far, very little is known about the structures that permanent magnetic chains may adopt as a function of temperature, length, and other related parameters like magnetic momentum of the particles, or the strength of the attractive interactions among colloidal particles.

In the case of non-magnetic attractive chains the study of their phase transitions has been exhaustive, see refs.^{31–37}, and refs.^{38,39} for a review. In the case of semiflexible attractive polymers it is known that there exist several conformational phases that are different from the typical swollen coils, collapsed globules, crystal and glassy states. Several works have reported semiflexible chains to exhibit toroidal or disk-like phases^{38,40–44}. Helix structures have also been found for some very specific square-well potentials⁴⁵. Related to it, helical long-lived transient states have also been identified for chains with truncated Lennard-Jones potentials⁴⁶.

For magnetic chains the number of studies is much lower. In addition to the previously mentioned works devoted to the experimental synthesis of magnetic filaments, there have been several attempts to obtain phase diagrams for magnetic chains using Ising or Heisenberg-like monomers in good solvent^{47–51}, corresponding to the case of non-attractive colloids. Henceforth, we will refer to such kind of chains as non-sticky filaments. In addition, some works have also dealt theoretically with the investigation of the magnetostatics of chains made of magnetic nanoparticles of different shapes⁵². The derivation of the partition function, the intra-chain correlations, and the coil-globule transition for flexible non-sticky magnetic chains in the limits of zero and infinitely strong external magnetic fields has also been pursued⁵³. A large fraction of the existing works has been devoted to the study of the properties of magnetic filaments made of paramagnetic or super-paramagnetic non-sticky chains. Most of these studies treat the filaments as elastic rods to use them as micro-propellers (microswimmers)^{4,25,54–61} under the action of an external field, or as actuators^{16,24} with the purpose of performing tasks similar to those of micrometric magnetic cilia^{62,63}, but at the nanoscale.

For lower dimensionalities, Sánchez et al.⁶⁴ have recently addressed via numerical simulations the adsorption and the

equilibrium conformations that result when a non-sticky magnetic filament is adsorbed on top of an attractive surface. In their work a preliminary phase diagram was sketched for those filaments as a function of the temperature and the strength of the surface attractive interaction. In the adsorbed regime two different states were observed: at low temperatures, closed-chain structures were found. Such closed-chains are more or less extended chains with the two ends at close contact. At larger temperatures, the chains showed open conformations that resemble those observed for ordinary non-magnetic adsorbed chains. An even more recent work from the same authors⁶⁵ has characterised the different structural regimes displayed by a non-sticky flexible magnetic filament immersed in a perfect solvent when varying the strength of the dipolar coupling parameter.

Other works related to the study of the structures adopted by single magnetic filaments, specially at low temperatures, are those devoted to the study of clusters of free particles that interact via Stockmayer potentials (Lennard-Jones plus point dipole potentials). Thus, for instance, Miller et al.⁶⁶ have found that clusters of particles interacting via Stockmayer potentials exhibit a rich variety of ground states that includes rings and different types of coils with several topological knots. The type of ground state exhibit by a cluster of Stockmayer particles was found to depend strongly on the dipole moment and the number of particles. Nonetheless, to our best knowledge, it is unknown if the conformations of single magnetic sticky filaments at low temperatures will shear some resemblance with the ground states found for Stockmayer clusters which lack of any permanent links between particles.

In this paper we investigate the influence of magnetic interactions on the phase diagram of sticky and non-sticky magnetic chains in three-dimensions via the use of extensive Langevin dynamics simulations. In Section 2 we describe the numerical model and the details of the simulations. In Section 3 we present and discuss our results which, in sake of clarity, we have split in three main parts. The first and second part are devoted to the discussion of the structures and phases that exist in the weak and the strong regime for the attractive interaction, respectively. In the third part, all the results are collected in order to build up a tentative phase diagram. Finally, a summary and a discussion of the conclusions are presented in Section 4.

2 Numerical Model

In order to investigate the behaviour of flexible magnetic filaments in the limit of infinite dilution we have performed numerical simulations in which a single magnetic filament is placed in a unbounded open space. The magnetic filament is modelled as a bead-spring chain made of a sequence of N magnetic beads (colloidal particles) of diameter σ_e , carrying

a point dipole $\boldsymbol{\mu}_e$ at their centre. Henceforth, the subindex e denotes the experimental values of the physical quantities we use. The absence of such subindex means the quantity is expressed in reduced units. We will use through all this work reduced units. Thus, for a length l_e its corresponding reduced value is $l = l_e/\sigma_e$. In the simulations, in sake of simplicity, the diameter of the colloidal particles is set to $\sigma = 1$, so all length scales are measured in units of this diameter.

Two different types of particles will be considered: non sticky particles, where the predominant interaction between particles is the steric repulsion due to the their cores; and sticky particles, in which in addition to the repulsion there exists an attractive pair-wise interaction among the particles. Henceforth we will refer to this last interaction as '*the LJ interaction*'. The attractive interaction between two particles i and j will be modelled via the following potential that combines the core repulsive part (cutoff $r_{cut} = 2^{1/6}\sigma$), and the attractive part ($r_{cut} = 2.5\sigma$),

$$U_{att}(r) = V_{tsLJ}(r, \sigma, 1, r_{cut} = 2^{1/6}\sigma) + V_{tsLJ}(r, \sigma, \epsilon, r_{cut} = 2.5\sigma) \quad (1)$$

where r is the distance between the centres of the particles i and j , i.e. $r = |\mathbf{r}_i - \mathbf{r}_j|$, and V_{tsLJ} is a truncated-shifted Lennard-Jones potential⁶⁷,

$$V_{tsLJ} = \begin{cases} U_{LJ}(r) - U_{LJ}(r_{cut}), & \text{for } r < r_{cut} \\ 0, & \text{for } r \geq r_{cut} \end{cases}, \quad (2)$$

where $U_{LJ}(r) = 4\epsilon[(\sigma/r)^{12} - (\sigma/r)^6]$. The LJ energy parameter ϵ , is given in units of the experimental well depth ϵ_e , and any energy U will be also referred to ϵ_e , i.e. $U = U_e/\epsilon_e$. In the same way we choose the Boltzmann constant to be $k = 1$ in reduced units, and therefore the reduced temperature is $T = k_e T_e/\epsilon_e$. The modulus of the dipole moments can be also expressed in the reduced system as: $\mu^2 = \mu_e^2/(4\pi\mu_{0,e}\sigma_e^3\epsilon_e)$. It should be noted that the soft-core and the attractive part have been implemented as in eq. (1) and not through a simple LJ potential because we want to ensure that the effective repulsion is roughly the same when different values of $\epsilon < 1$ are used. In this way a comparison between chains with different depths for the attractive well and non-sticky chains can be performed more easily.

The colloidal particles are assumed to interact pair-wise as point dipoles according to the potential,

$$U_{dip}(\mathbf{r}_{ij}) = \frac{\boldsymbol{\mu}_i \cdot \boldsymbol{\mu}_j}{|\mathbf{r}_{ij}|^3} - \frac{3[\boldsymbol{\mu}_i \cdot \mathbf{r}_{ij}][\boldsymbol{\mu}_j \cdot \mathbf{r}_{ij}]}{|\mathbf{r}_{ij}|^5}, \quad (3)$$

where $\mathbf{r}_{ij} = \mathbf{r}_i - \mathbf{r}_j$ is the displacement vector between particles i and j . The energy due to magnetic interactions is calculated by direct summation over all pairs of particles. In spite of being algorithmically $\mathcal{O}(N^2)$, for small numbers of colloids this is the fastest and most accurate way to compute it due to

the open boundary conditions. The values of $\mu = |\boldsymbol{\mu}|$ to be used depend in general on the composition and size of the colloidal particles: aside from cobalt nanoparticles, colloidal particles found in common commercial ferrofluids usually do not exceed values of $\mu \sim 10$.

In order to connect the colloids to form a chain, a linking model for the particles slightly more involved than the one used in previous works^{64,65} has been implemented. In this new approach springs between consecutive particles are not anchored at the centres of the beads, but at fixed points on their surface, as shown schematically in Figure 1. The reason to implement a novel variant of the bead-spring model is to better mimic the real behaviour of magnetic filaments made of sticky colloidal particles. In our preliminary tests using springs anchored at the centre of the dipoles, we noticed that, for moderate and strong magnetic coupling, the sticky filaments form packed structures holding filament sections in which the dipole orientation is inverted with respect to the chain backbone in order to minimize the overall magnetic energy. Nonetheless, in most common real magnetic filaments, those inversions would imply a strong stretching of the bond linking the colloidal particles at the borders of the two different domains. Thus, the existence of such inverted domains in real filaments must be heavily penalised. Instead, chains modelled with springs anchored at fixed points on the surface of the beads, penalise such 180 degrees rotations in an effective way. The model we present is therefore useful to analyse the behaviour of particles with permanent magnetic moment, i.e. those that having a magnetic monodomain that is blocked in the crystal structure of the particle and in consequence the dipole is only allowed to relax via the Brownian mechanism.

The proposed spring potential is written as:

$$U_s(\mathbf{r}_i, \mathbf{r}_j, \hat{\mathbf{u}}_i, \hat{\mathbf{u}}_j) = \frac{1}{2}K_s \left(\mathbf{r}_i - \mathbf{r}_j - (\hat{\mathbf{u}}_i + \hat{\mathbf{u}}_j) \frac{\sigma}{2} \right)^2, \quad (4)$$

where \mathbf{r}_i and \mathbf{r}_j are the position vectors of the centres of the beads. $\hat{\mathbf{u}}_i$ and $\hat{\mathbf{u}}_j$ are unitary vectors placed along the direction that joins the two anchoring surface points of each bead (see figure 1). Thus, the anchoring points are collinear and located at $\mathbf{l}'_i = \hat{\mathbf{u}}_i\sigma/2$ and $\mathbf{l}_i = -\hat{\mathbf{u}}_i\sigma/2$ with respect to the centre of the bead. We assume all links in the chain are formed according to the following scheme: the point on the surface of the $i-1$ particle with position $\mathbf{r}_{i-1} + \mathbf{l}'_{i-1}$ is linked to the point on the surface of the particle i with position $\mathbf{r}_i + \mathbf{l}_i$. In order to obtain the desired effect of severely penalising conformations with consecutive dipoles in anti-parallel configuration, we associate each director vector $\hat{\mathbf{u}}_i$ with the dipole moment of the particle, $\boldsymbol{\mu}_i$, i.e. $\hat{\mathbf{u}}_i = \boldsymbol{\mu}_i/|\boldsymbol{\mu}_i|$. The constant of the potential is set to $K_s = 30$ which is enough to ensure the average bond length to lie within a reasonable range $r_{bond} \in [0.98, 1.1]\sigma$. The use of larger values for K_s is possible but implies a further reduction of the integration time step.

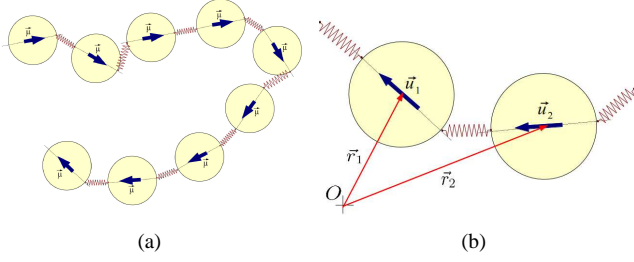


Fig. 1 The magnetic filament is modelled as a chain of beads linked by springs anchored onto a point of their surfaces, see eq. (4). The magnetic moment of each particle is used as reference vector to define the unitary vectors $\hat{\mathbf{u}} = \boldsymbol{\mu}/\mu$ which are used to determine the position of the anchoring points on the surface of the particles, $\sigma/2 \hat{\mathbf{u}}$ and $-\sigma/2 \hat{\mathbf{u}}$, when the centre of the particle is taken as the origin.

The numerical simulations are performed using Langevin dynamics, in which colloidal particles are moved according to the translational and rotational Langevin equations of motion that for a given particle i are⁶⁸:

$$M_i \frac{d\mathbf{v}_i}{dt} = \mathbf{F}_i - \Gamma_T \mathbf{v}_i + \boldsymbol{\xi}_i^T \quad (5)$$

$$\mathbf{I}_i \cdot \frac{d\boldsymbol{\omega}_i}{dt} = \boldsymbol{\tau}_i - \Gamma_R \boldsymbol{\omega}_i + \boldsymbol{\xi}_i^R \quad (6)$$

where \mathbf{F}_i , and $\boldsymbol{\tau}_i$ are respectively the total force and torque acting on the particle i , M_i and \mathbf{I}_i are its mass and inertia tensor while Γ_T and Γ_R are the translational and rotational friction constants. $\boldsymbol{\xi}_i^T$ and $\boldsymbol{\xi}_i^R$ are Gaussian random forces and torques, each of zero mean and satisfying the usual fluctuation-dissipation relations. In the simulations, $t = t_e \sqrt{\varepsilon_e / (m_e \sigma_e^2)}$, where m_e is the real mass of the colloids; $F = F_e \sigma_e / \varepsilon_e$, and $\tau = \tau_e / \varepsilon_e$. For equilibrium simulations, the values of the mass, the inertia tensor, as well as friction constants Γ_T , and Γ_R are irrelevant because the same equilibrium state is reached independently of their value. Only the dynamics to attain such equilibrium state may show differences. Thus, in sake of simplicity, the particle mass is chosen to be $m = 1$ and we take the inertia tensor to be the identity matrix in order to ensure isotropic rotations $\mathbf{I} = \mathbf{1}$. We have chosen $\Gamma_T = 1$ and $\Gamma_R = 3/4$ because we observed that these values produced a conveniently fast relaxation to equilibrium^{69,70}. The reduced time step is set to $\delta t = 5 \cdot 10^{-4}$ in order to ensure a correct integration of the equations of motion.

The simulations are started by placing the filament in a open three-dimensional non-bounded space with the position of the first bead located randomly. The remaining monomers are positioned using a self-avoiding random walk scheme with an overlap radius of 0.9σ . The chain is pre-equilibrated at $T = 1$ for $2 \cdot 10^5$ integrations with the magnetic interaction turned

off while the time step is slowly increased from $10^{-3}\delta t$ till $0.05\delta t$. Subsequently, magnetic interactions are turned on, and a second pre-equilibration stage consisting of $5 \cdot 10^5$ integrations is performed while gradually raising the time step from $0.1 \cdot 10^{-3}\delta t$ till δt . Right after, if the final temperature is $T < 1$ we perform an annealing process using the final time step δt : the temperature is reduced from $T = 1$ down to its final value by performing a set of five annealing stages of $5 \cdot 10^5$ steps each one. Once the final temperature has been reached, the chain is equilibrated for a period of $3 \cdot 10^6 e^{1/T} \delta t$ in order to ensure that the chain is in the thermodynamic equilibrium. After the equilibration period, the system is sampled at intervals of $2500 e^{1/T} \delta t$ for another period of $15 \cdot 10^6 e^{1/T} \delta t$ to make sure there are no correlations between measurements. To get further assurance that the results do not depend on the initial conditions and to improve statistics, an average over 15 independent runs for each set of sampled parameters (T, ε, μ) is performed. The simulations have been performed using the package ESPResSo⁷¹.

3 Results and discussion

In the present model there are two main competing interactions: on the one hand there is the LJ attractive interactions among the beads that tend to collapse the chain when the temperature is lowered^{38,39}; on the other hand there is the magnetic interaction which is known from ferrofluid studies^{69,70} to favour the formation of rod-chains and rings in which dipoles tend to align in a nose-tail conformation. Nose-tail conformations are those in which two dipole i and j satisfy $\boldsymbol{\mu}_i \cdot \boldsymbol{\mu}_j = \mu^2$, and $\boldsymbol{\mu}_i \cdot \mathbf{r}_{ij} = \boldsymbol{\mu}_j \cdot \mathbf{r}_{ij} = \pm \mu r_{ij}$. This nose-tail alignment allows to minimise the magnetic energy in eq. (3). Thus, it seems reasonable to define the dimensionless parameter $\eta \equiv \frac{\varepsilon \sigma^3}{\mu^2}$ which measures the relative strength of the attractive LJ interaction compared to the strength of the magnetic interaction for particles at close contact, $r_{ij} = \sigma$, in a nose-tail conformation.

Although we just focus on the behaviour of a single chain, the number of parameters involved to explore the full phase diagram is large. Therefore, in order to get a first sketch on a section of the the phase diagram, we have chosen to focus on a specific case with a fixed number of beads $N = 100$. In addition, all beads are assumed to have the same magnetic moment $\mu^2 = 5$ and share the same LJ energy parameter ε . In this first approach no external magnetic field is present. The phase diagram will be studied as a function of two parameters: η , that is controlled modifying the value of ε while keeping μ fixed, and the temperature T . The range of values explored for the parameter η is $\eta \in [0, 0.2]$. $\eta = 0$ corresponds to the case in which particles do only exhibit sterical repulsion between their cores and no effective attractive LJ interaction ex-

ist among them (non-sticky filaments). This case is quite common when magnetic particles are sterically stabilised against flocculation, as is the case of ferrofluids⁷². The range of temperatures sampled is $T \in [0.27, 5]$, where the upper boundary $T = 5$ has been chosen because the most interesting features were found to occur well below such value in all cases. The relative strength of the magnetic to the thermal energy, is usually expressed in terms of the dipolar coupling parameter λ , which is defined as half of the ratio of the magnetic energy of two dipoles in close contact and in a nose-tail alignment to the thermal energy, *i.e.* $\lambda = \mu^2 / (Tr_{bond}^3)$. Thus, the value of the effective dipolar coupling parameter for the systems under study ranges in $\lambda \in (0.6, 20)$, being $\lambda \approx 10$ for $T = 0.5$, and $\lambda \approx 1$ for $T = 3.5$. Nonetheless, even at $T = 5$ the thermal motion is still not powerful enough as to completely overcome the magnetic interactions: the main structural observables of the chain have values still far from those corresponding to an ideal self avoiding random walk that is the behaviour one could expect in the limit $T \rightarrow \infty$. Nonetheless, once the chain is in an extended open state, we do not expect any other relevant change to happen by raising T .

Values of $\eta > 0.2$ and $T < 0.27$ correspond to regions in the phase space characterised by compact structures. An effective sampling of these regions with usual Langevin methods is very costly in computer terms and require special techniques like *e.g.* umbrella sampling⁶⁸, Wang-Landau method^{73,74} or other advanced existing methods^{32,35}, and is left for future work, although our preliminary results suggest the existence of interesting features that are worthwhile to be explored⁷⁵.

In sake of a better understanding we have split the discussion of the results in three parts. In the first part we will discuss the behaviour of the magnetic filaments for $\eta < 0.10$, in the second part for $\eta \geq 0.10$ and in the third and last part we will discuss the implications our results have for the phase diagram of magnetic filaments.

3.1 Filaments with $\eta < 0.10$

The radius of gyration R_g and the end-to-end distance R_{ee} are two important observables that can be very useful in order to follow the structural changes of a magnetic filament. The end-to-end distance is defined as $R_{ee} = \langle (\vec{r}_1 - \vec{r}_N)^2 \rangle^{1/2}$ where $\langle \dots \rangle$ denotes an average over all the sampled conformations of the chain. On the other hand, we can define the *gyration tensor* through their elements,

$$R_{\alpha,\beta} = \frac{1}{2N^2} \left\langle \sum_{i,j=1}^N (r_{i,\alpha} - r_{j,\alpha})(r_{i,\beta} - r_{j,\beta}) \right\rangle \quad (7)$$

where α and β denotes de Cartesian components x , y , and z . The tensor can be represented as a diagonalisable 3×3 matrix with three eigenvalues or principal moments hence-

forth labelled as $\lambda_1^2 > \lambda_2^2 > \lambda_3^2$. The radius of gyration is $R_g = \sqrt{\lambda_1^2 + \lambda_2^2 + \lambda_3^2}$.

Figure 2 shows the end-to-end distance (top plot) and the gyration radius (bottom plot) as a function of the temperature. Our results show that the ends of the chain tend to get closer as the temperature is lowered. Remarkably, the behaviour of the end-to-end distance is very similar for all filaments with $\eta \in [0, 0.07]$. In the range $\eta > 0.07 - 0.10$ a noticeable two-fold decay step emerges whose origin is explained below.

Also, as can be observed in figure 2, the radius of gyration of sticky filaments ($\eta > 0$) shows a progressive difference, when compared with non-sticky filaments ($\eta = 0$). For all measured values of $\eta > 0$, the magnetic filaments tend to shrink when there is an attractive LJ interaction among the beads. As in the case of the end-to-end distance, the radius of gyration also tends to develop a two-fold decay for $\eta \rightarrow 0.10$.

In the case of non-sticky particles, $\eta = 0$, the variation in the values of R_g is quite small. It ranges from a value of $R_g \sim 9\sigma$ at $T = 5$ (value not shown in the figure 2) to a value of $R_g \sim 12\sigma$ at $T \sim 0.3$. Nonetheless the behaviour of R_g is clearly different from the one expected for non-magnetic chains: for such chains without attractive interactions, one would expect R_g to be approximately constant if the bond length is fixed. Here, as the temperature is lowered, the magnetic filaments show an initial expansion, followed by a contraction $T \in [0.7, 1.0]$ and a second expansion at $T < 0.7$. This particular behaviour is also observed in filaments with values of η closer to $\eta = 0$ down to a temperature in which the attractive interactions dominate and induce a strong collapse of the chain. This expansion-contraction behaviour can be understood as follows: as the temperature is lowered the magnetic interactions for an extended open chain dominate, and favour the stretching of the chain in a conformation in which all the dipoles tend to remain aligned along the same direction. Nonetheless, below a certain temperature, the most favourable conformation is a closed structure because an extra aligned pair can be created by getting closer the ends of the chain. The entropic penalty of a closed chain is not excessive when the temperature is low enough. The closed structures at low temperatures are already known to occur in ferrofluids⁷⁶, where particles assemble into ring-like structures. Although the tendency is to form a ring when the temperature is lowered, the structure of the filament is far from being a perfect ring at the point where the filament closes. This can be observed in the plots corresponding to $\eta = 0$ in figure 3. An additional proof in favour of this relation between the closing of the chain and the slight decay of the radius of gyration is the fact that both phenomena occur in the same range of temperatures (see figure 2). For low values of η the transition from open to closed structures occurs at $T \sim 0.85$, which corresponds to a value of the dipolar coupling parameter of $\lambda \sim 6$. These results are in

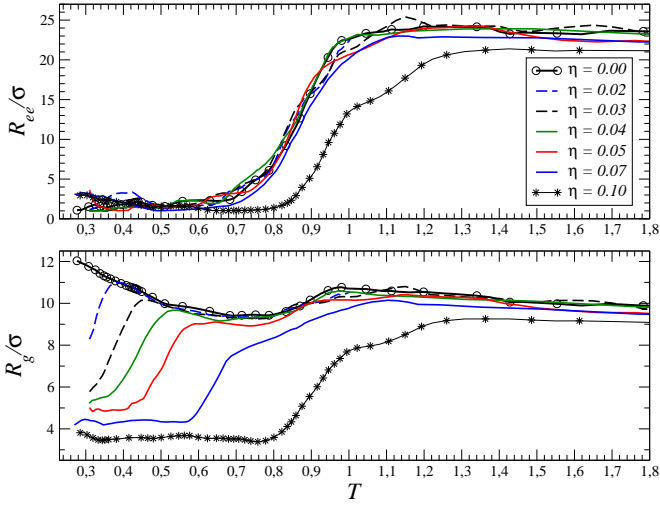


Fig. 2 The plot depicts the the end-to-end distance R_{ee} (top) and the radius of gyration R_g (bottom) as a function of the temperature for $\eta < 0.10$. The case $\eta = 0.10$ has been also included for a better comparison with the results corresponding to $\eta > 0.10$.

good agreement with what has been observed for non-sticky chains in the simpler variant of the bead-spring model⁶⁵.

Further insight on the behaviour of the magnetic filaments in the regime $\eta < 0.10$ can be obtained by examining the specific heat C_V , defined in terms of our dimensionless temperature as

$$C_V = \frac{\langle U^2 \rangle - (\langle U \rangle)^2}{T^2}, \quad (8)$$

where U is the total energy of the filament [$U = U_{att} + U_{dip} + U_S$]. The experimental specific heat is related to this definition according to $C_{Ve} = k_e C_V$. Figure 4 shows the specific heat as a function of temperature. The bottom plot in figure 4 shows some small peaks appearing around $T \sim 0.8 - 0.9$ which can be identified with the transition from open to closed structures. Three main features can be observed for such peaks: the first one is that for values of $\eta \in [0, 0.07]$ they almost coincide in position, value and width. This means that the corresponding transitions are almost independent of the strength of the attractive interaction. This independence is due to the absence of close contacts between particles which are not first nearest neighbours. The second feature is that compared to the peaks that can be observed in the top plot of figure 4, the peaks around $T \sim 0.8 - 0.9$ represent very small fluctuations in the energy. This fact is coherent with the idea that those peaks represent a transition from extended open to simple closed structures because the difference in the total energy between one state and the other should not be much larger than the energy due to the creation of a new pair of aligned dipoles, plus the energy due to the close contact of two particles. A third

feature is that when the value of η increases, the peaks representing the transition from open to closed structures become partially overlapped by the tails of the larger peaks present in the specific heat. This overlap makes it very difficult to determine the temperature of the open-closed transition from the peaks of the specific heat for values of $\eta > 0.07$. In fact, the only observable we have found to roughly determine the point of this transition is $dR_{ee}(T)/dT$. It is reasonable to consider that the transition approximately coincides with the inflection point of the end-to-end distance, *i.e.* $dR_{ee}(T)/dT$ has an extrema at that temperature. Nonetheless the scenario becomes more complex due to the fact that, as $\eta \rightarrow 0.10$, R_{ee} shows a two-fold decay. We will come back to this point later in section 3.3 where a global picture of the phase diagram will be available.

The large peaks observed in the specific heat in figure 4 represent a different type of transition, namely, the conversion of the simple closed structures into compact helicoidal-like structures as it can be observed in figure 3 for snapshots at $\eta = 0.05$ and $T < 0.6$. As it is shown in figure 5 the main part of the filament adopts a structure that remembers a tight helix, while the ends of the chain arrange in such a way that the two ends stay in close contact. These helicoidal states are related to the toroidal conformations observed in non-magnetic semi-flexible chains where local chain stiffness helps to stabilise those structures^{38,43}. In our case, the magnetic interactions tend to force a nose-tail orientation of the dipoles that, in addition, will induce a local chain stiffness⁶⁴. Nonetheless, there are some subtle differences between the toroidal conformations found in non-magnetic chains and the helicoidal structures observed here: in the non-magnetic case the toroidal walls are thick with a width of several particle diameters while in the magnetic case they tend to be much thinner. An open question is what would happen if longer chains of the order of $N \sim 10^3 - 10^4$ were studied. We argue that in the case of magnetic chains, an helicoidal state is preferred to a toroidal conformation, at least if η is not very large. An helicoidal structure allows to minimise the energy associated to pairs of dipoles with their dipole moments lying parallel $\boldsymbol{\mu}_1 = \boldsymbol{\mu}_2 \equiv \boldsymbol{\mu}$ but for which $\mathbf{r}_{12} \cdot \boldsymbol{\mu} = 0$. Unlike the nose-tail conformations, these pairs have the highest possible magnetic energy and therefore are heavily penalised. Such energy penalty decreases as $\sim 1/r^3$ with the distance between the two dipoles. In a toroidal conformation, a similar number of unfavourable dipole pairs may exist, but in difference to the helicoidal structure the distance between the two particles will be, in general, much shorter, leading to a higher energy penalty. The situation reverts for large values of η in which the short ranged attractive interaction dominates over the magnetic one and a torus is preferred. Thus, helicoidal structures seem to be the result of a complex interplay between the attractive interactions that tend to collapse the chain into an isotropic globule, the mag-

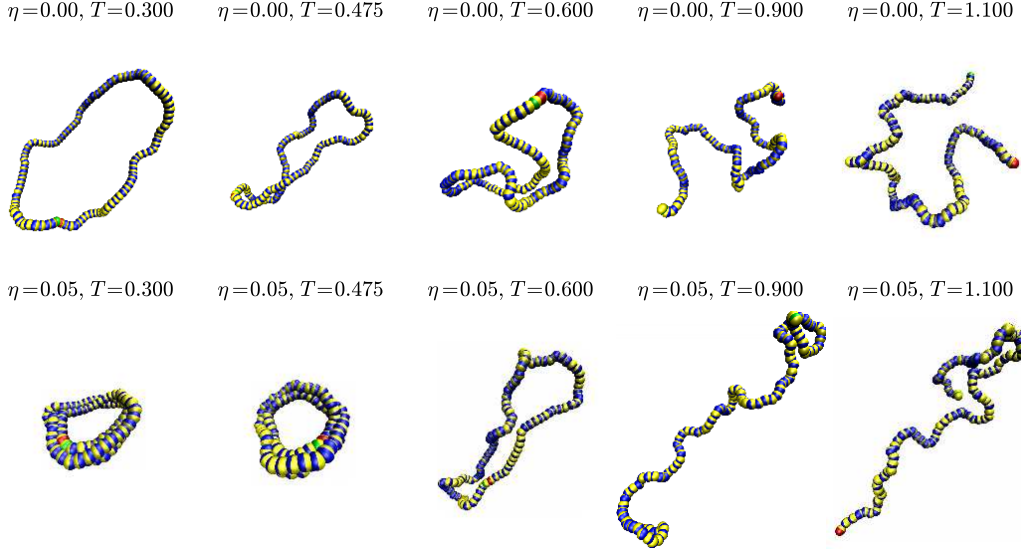


Fig. 3 The figure depicts several typical snapshots of the configurations that magnetic filaments of length $N = 100$ adopt for different values of the temperature and relative strength of the attractive interactions η . Snapshots for $\eta = 0, 0.05$ are shown. The two ends of the filaments are shown in green and red colours. The rest of the beads are painted in two colours (yellow and blue) to show the orientation of the magnetic moments of the particles.

netic forces which, on the one hand, tend to locally stretch the chain by leading to an effective local stiffness that favours toroidal conformations but, on the other hand, tend to avoid the formation of pairs of parallel dipoles with their relative vector position perpendicular to the direction of the dipoles, and the chain entropy. It is also worth to mention that helicoidal states have been found for non-magnetic chains when specific short-ranged square-well potentials were used⁴⁵. Another issue worth to mention is the possibility that those helicoidal states could be long-lived metastable transient states as those found by Sabeur et al.⁴⁶ for simple homopolymers using truncated Lennard-Jones potentials whose monomers were subject to simple spring potentials anchored on their centres. Since we use similar reduced units, and share the same simulation technique (Langevin dynamics), a rough comparison is feasible: Sabeur et al. observed that the decay from the helical states is a stochastic rate-driven process, where the escape rate is $1/t_o \sim \exp(\Delta E/kT)$ and ΔE is the height of the energy barrier. In their simulations they found a value of $t_o \approx 2000\delta t$ for the particular case of a homopolymer chain of length $N = 100$ at $T = 0.04$. Since our equilibration and measurement times are of the order of $3 \cdot 10^6 e^{1/T} \delta t$ and $15 \cdot 10^6 e^{1/T} \delta t$ respectively, and taking into account that the lowest temperature we have sampled is of the order of $T \sim 0.25$, we can reasonably conclude that the helicoidal structures we observe are not expected to be long-lived metastable states but true equilibrium

states.

Figure 4 shows that the peaks in the specific heat signalling the formation of the helicoidal states are much larger than those related to the extended open to simple closed structure transitions. This fact is a consequence of the substantial increase in the number of particles at close contact that appear in the helicoidal state with respect to the simple closed structures, in which the main interactions are only between the nearest neighbours in the chain sequence and between the chain ends. The global chain rearrangements show up as large fluctuations in the total energy, and thus, larger peaks in the specific heat are expected. Another feature of the helicoidal transition is that the transition temperatures in this case show a strong dependence with η , which is quite opposite to the behaviour observed for the transition from extended open to simple closed structures where the transition temperature remains almost invariant.

It is worth to remark that, within the range of sampled temperatures, peaks associated to such transition are only observed for $\eta > 0.02$. We expect such helicoidal transitions to take place also at $\eta \leq 0.02$ and smaller temperatures ($T < 0.27$). A question that remains open is whether the transition from simple closed to helicoidal conformations takes place for all non-zero values of η , or if there is a critical value for the strength of the attractive interaction, η_c , such that for $\eta < \eta_c$ the closed-helicoidal transition is not possible.

A quantitative way to characterise the formation of an helicoidal state is to evaluate a typical order parameter able to signal the formation of an helix. Among the different order parameters⁴⁶, we have chosen the so-called H_4 parameter which characterises the global helical order defined as

$$H_4 = \frac{1}{N-2} \left\langle \sum_{i=2}^{N-1} (\mathbf{r}_i - \mathbf{r}_{i-1}) \times (\mathbf{r}_{i+1} - \mathbf{r}_i) \right\rangle. \quad (9)$$

$H_4 = 0$ is associated to isotropic conformations that resemble a rod, whereas $H_4 = 1$ holds for perfect helix. Other order parameters like H_3 ⁷⁷ were found to lead to similar conclusions that those derived from H_4 .

In figure 6 (top plot) the value of the order parameter H_4 as a function of the temperature is depicted for $\eta \leq 0.10$. The values of H_4 remain equal to zero until temperatures close to the helicoidal transition point. The derivative, dH_4/dT , shows that the position of the inflection points occurring at the highest temperature coincides with the position of the peaks in the specific heat. This fact shows that both observables are linked to the appearance of helicoidal states. Figure 6 shows that the achievement of the helicoidal states is very gradual: the further the temperature is lowered the higher is the value of H_4 , and the structure looks more similar to a perfect helix. Only for values of $\eta \rightarrow 0.10$, the order parameter H_4 seems to reach a plateau within the range of temperatures sampled. In any case, the largest values of $H_4 \sim 0.4$ are quite low compared with those of an ideal helix $H_4 = 1$. These relatively small values for the order parameter have a two-fold cause: the first one is that only the main part of the chain adopts an helix-like structure, whereas the ending parts of the chain arrange in such a way that the ends can be at close contact. If the whole structure was in an helicoidal state the two ends would be separated by a large distance, which gives an energy penalty. Such small differences in energy may be irrelevant at high temperatures but not at low temperatures. The second reason lies in the fact that these helicoidal states do not look like normal cylinders but rather they exhibit a symmetry similar to that of an elliptic cylinder, whereas the parameter H_4 is defined having in mind ideal helixes with a symmetry similar to that of a regular cylinder. Notice that the cross product $(\mathbf{r}_i - \mathbf{r}_{i-1}) \times (\mathbf{r}_{i+1} - \mathbf{r}_i)$ would be zero for a very elongated ellipse in which bonds between particles are locally aligned.

The asymmetry of the filaments can be roughly inferred from a visual inspection of the different conformations shown in figure 3. However, a good set of observables to determine quantitatively the degree of asymmetry of the different conformations are the ratios of the second and third eigenvalues of the gyration tensor to the main eigenvalue, λ_2^2/λ_1^2 and λ_3^2/λ_1^2 . Those ratios are shown in 7 as a function of temperature. In the region of high temperatures $T \in [1.8, 5]$ the ratios of the eigenvalues are approximately constant and equal to $\lambda_2^2/\lambda_1^2 \sim 0.2$

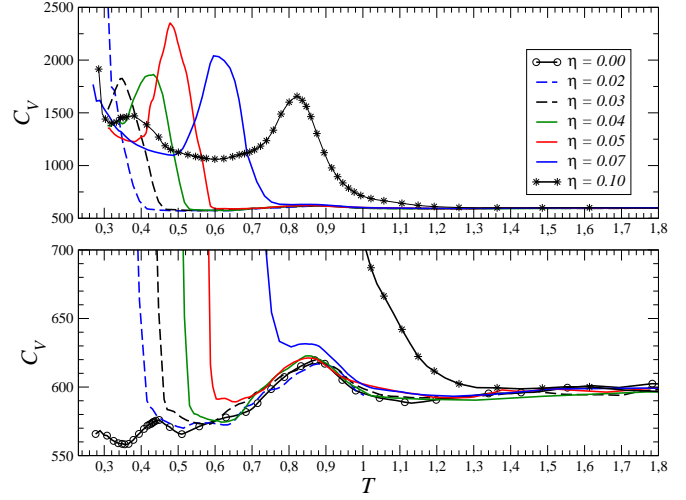


Fig. 4 The specific heat as defined in eq. (8) is represented as a function of temperature for different values of the relative strength of the LJ attractive interactions η . The bottom plot is a zoom to highlight the small peaks that exist at $T \sim 0.8 - 0.9$ which point out the transition from extended open chains to simple closed structures.

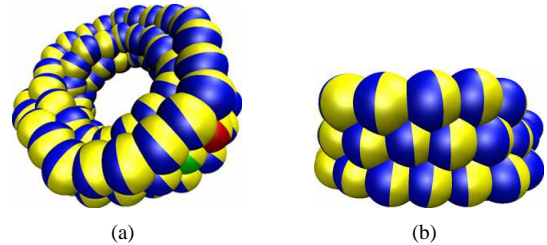


Fig. 5 The figure depicts two different perspectives of a typical conformation in the helicoidal state ($\eta = 0.10$, and $T = 0.475$). The code of colours follows from figure 3.

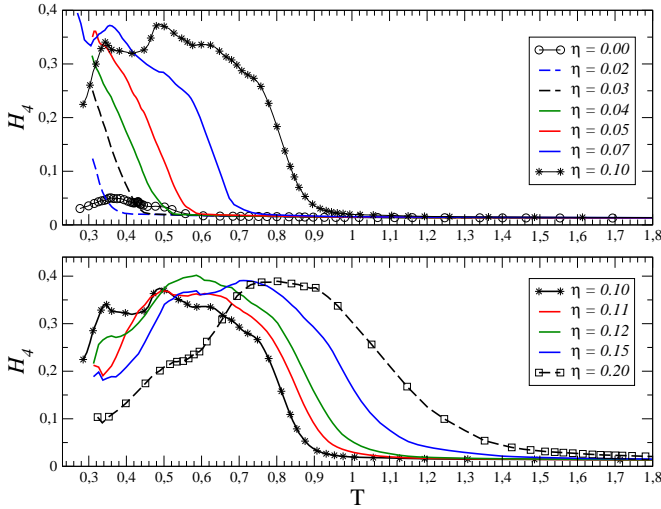


Fig. 6 The helicoidal order parameter H_4 as defined in eq. (9) is plotted as a function of temperature for several values of $\eta \leq 0.10$ (top plot) and $\eta \geq 0.10$ (bottom plot).

and $\lambda_3^2/\lambda_1^2 \sim 0.06$, respectively. These ratios mean that filaments are highly elongated along one direction and almost lie in a plane because the value of third eigenvalue is almost negligible respect the first and second eigenvalues. These behaviour roughly corresponds to the tendency of the magnetic particles to align themselves in a row. The fact that the value of the ratios is almost the same for all $\eta \leq 0.10$ implies that in the range of high temperatures the attractive interaction plays a very minor role. Nonetheless, we are still far from the limit $T \rightarrow \infty$ where we expect to observe filaments with values of the eigenvectors that resemble those of an ideal SAW with $\lambda_1^2 = \lambda_2^2 = \lambda_3^2$.

Another interesting feature is that the eigenvalue ratios for $0 < \eta < 0.07$ are almost identical to the case $\eta = 0$ up to the helicoidal transition takes place. This implies that in the transition from simple closed to helicoidal states, the shape of the closed structures for sticky filaments with $\eta \in (0, 0.07)$ is similar to that of simple closed structures formed by non-sticky filaments at the same temperature. In the region where helicoidal structures exist, a comparison between the sticky filaments with the non-sticky ones ($\eta = 0$) shows that the attractive interaction, as it could be expected, favours the more isotropic structures.

A comparison of figures 7 and 2 shows that the temperature at which the eigenvalue ratios separate from the non-sticky case coincides with the temperature at which R_g suffers a more prominent decay. Thus, when the chain collapses by reducing its size in every direction, the global shape becomes more symmetric.

In the region where compact helicoidal structures exist, the

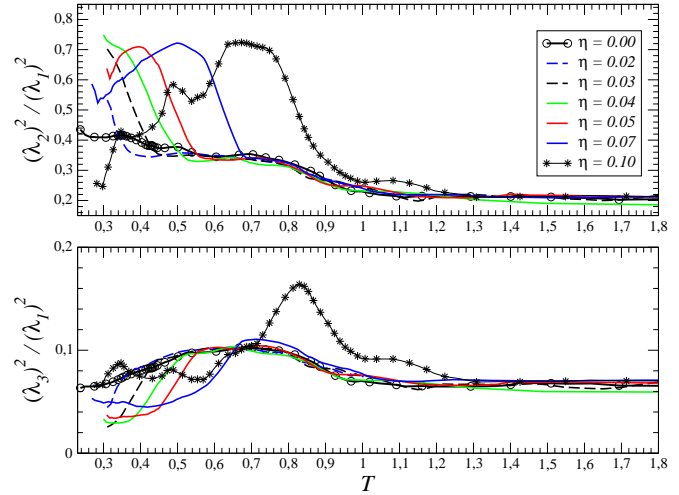


Fig. 7 The ratio of the second and third eigenvalues of the gyration tensor, see eq. (7), to the main eigenvalue are shown as a function of the temperature for several values of $\eta \leq 0.10$.

second eigenvalue exhibits a substantial increase, $\lambda_2^2/\lambda_1^2 \sim 0.74$, which shows that the helicoidal states do not project on top of a circle but rather of an ellipse. This fact is consistent for all the values of η sampled. Below a certain temperature, the degree of anisotropy of the shapes of the filaments gradually increases again, a signal that points in the direction that another conformational phase is arising. We shall come back to this point in section 3.2.

At first sight, it can be surprising that all closed and collapsed structures do not show, in average, an isotropic distribution of particles, at least along their two main axis of rotation. This can be understood as follows: in addition to an ideal distribution of N particles over a circumference with their dipole moments tangent to the curve, there exist other closed structures which are non isotropic and have an energy that is comparable to that of an ideal circumference. One should expect the system at finite T to sample different states of similar energy, and consequently, the averaged values of the eigenvalues of the gyration tensor should also reflect a certain degree of anisotropy. In addition we should take into account that bonds between particles are not constant, but fluctuate around their mean value which can further enhance the number of anisotropic states with energies similar to those of a ring conformation.

3.2 Filaments with $\eta \geq 0.10$

As we have already shown in figure 4, the specific heat develops an additional peak for $\eta = 0.1$ at $T \sim 0.4$. This peak is also observed for $\eta > 0.1$ (see top of figure 8) and, as $\eta \rightarrow 0.2$, it shifts towards higher temperatures $T \in [0.3, 0.7]$ while de-

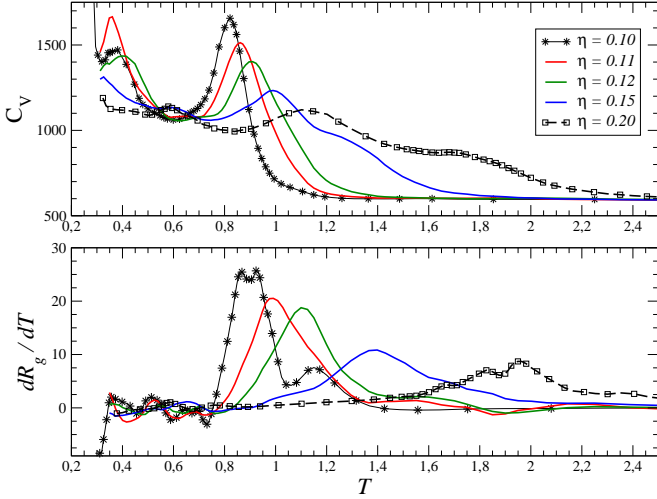


Fig. 8 The figure depicts in the top plot the specific heat as a function of the temperature for several values of the relative strength of the attractive interaction $\eta \geq 0.10$. The bottom plot shows the derivative of the gyration radius dR_g/dT as a function of the temperature for the same range of η 's.

creases in height. The radius of gyration and the end-to-end distance depicted in figure 9 show that those peaks in the C_V must correspond to a transition that takes place when the chain is already in a collapsed state. For that reason it is very difficult to discern from the structural parameters any relevant signal of the transition. This transition must involve an internal rearrangement of the particles without noticeable changes in the global size of the structure. A rough idea of such internal rearrangements is provided by the helical order parameter H_4 depicted in the bottom plot of figure 6 for $\eta \geq 0.10$. A comparison between C_V and H_4 (top of figure 8) reveals that the inflection point of the H_4 lines in the interval $T \in [0.3, 0.7]$ roughly coincides with the position on the peak in the specific heat. We can infer that the new transition is associated with a loss of the helicoidal order and the onset of compact disordered states. A typical structure in this regime is represented in figure 10a.

The knowledge of the eigenvalues allows to make a rough estimation of the volume that the magnetic filament occupies if an assumption about the shape of the filament is made. For the most compact case studied, that corresponds to $\eta = 0.2$ in the low temperature regime ($T \in [0.3, 0.6]$), we found the eigenvalues of the gyration tensor to be approximately $\lambda_1^2 \sim 4$, $\lambda_2^2 \sim 2$, and $\lambda_3^2 = 1$. The ratios of the eigenvalues as well as the snapshots of the systems at such temperatures suggest that plausible shape for the filament is an elliptic cylinder. Under this assumption, the major semi-axis is $a \approx \sqrt{(3)} + 1$, the minor semi-axis is $b \approx \sqrt{(15)} + 1$ and the height is $h \approx \sqrt{(3)} + 1$.

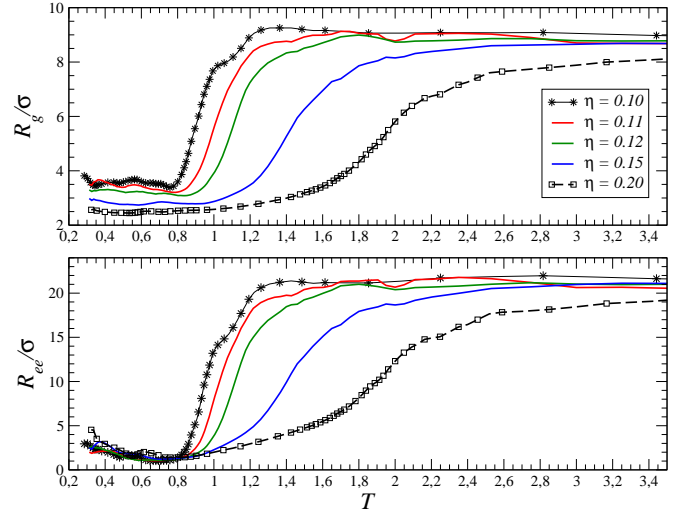


Fig. 9 The radius of gyration (top plot) and the end-to-end distance (bottom plot) are depicted as a function of temperature for several values of the relative strength of the attractive to the magnetic interaction η .

The correcting factor $+1$ is added because the gyration tensor only takes into account the centre of the particles, and the calculated elliptic cylinder will neglect about half of the volume of the most outer particles. Once the parameters of the elliptic cylinder are known, the calculation of the approximate volume of the elliptic cylinder is straightforward: $V_c = \pi abh \approx 114\sigma^3$. To get an idea of the degree of compaction achieved, we should compare the previous volume to that of a compact hexagonal packaging (hcp) of $N = 100$ spheres, $V_{hcp} \approx 74\sigma^3$. This result shows that the magnetic filaments at $\eta = 0.2$ and $T < 0.6$ exhibit a degree of compaction close to that of a hcp lattice of impenetrable spheres. On the other hand, for $\eta > 0.1$ we observe that the helicoidal structures developed are far more isotropic than for $\eta < 0.1$. Thus, for $\eta = 0.2$ the highest ratios of the eigenvalues are $\lambda_2^2/\lambda_1^2 \sim 0.9$ and $\lambda_3^2/\lambda_1^2 \sim 0.6$ that imply a significant increase in the level of isotropy when compared to those values for $\eta < 0.1$ that are plotted in figure 7.

From the comparison among C_V , R_g and R_{ee} for $\eta \geq 0.1$ we can extract more useful information about the magnetic chains. A remarkable feature in figure 9 is that R_g and R_{ee} have a very similar dependence with the temperature. This result differs from the observed behaviour for $\eta < 0.10$ in which the filament first suffers a closing transition as T is lowered and only then, by further reducing the temperature, there is a collapse of the chain towards a compact helicoidal state, *i.e.* the end-to-end distance decays at higher temperatures than R_g does. However, for $\eta \geq 0.10$, the attractive interaction is strong enough to force compaction to occur at higher temper-

atures than those at which filaments would suffer the closing transition. In principle, the closing temperature should not be substantially modified respect to the value for the non sticky case because the value of the magnetic dipoles is kept constant. Nonetheless, once the compaction of the chain occurs, the distance between the chain ends must substantially decrease, and this lets the closing transition to occur right after the compaction.

Another remarkable feature that can be extracted from figure 9 is the observation that for the curves corresponding to $\eta = 0.15$ and $\eta = 0.20$ it is possible to clearly associate the inflection points in $R_g(T)$ with the two emerging peaks in the specific heat (figure 8 top) at $T \sim 1.3 - 1.4$ and $T \sim 1.8 - 1.9$, respectively. This behaviour suggests the existence of a regime of intermediate states between the expanded chains and the compact helicoidal configurations. For values of $\eta \in [0.10, 0.15)$ one can infer that the peak is also present but hidden in the long tail associated to the appearance of helicoidal states that take place in the interval $T \in [0.8, 1.1]$. For these smaller values of η the fingerprint of the transition towards this intermediate regime is found in the double stage decay of both R_{ee} and R_g (figure 9). A natural question that arises is what kind of conformations do exist in such intermediate region. The plots of R_g and R_{ee} in figure 9 show that for those intermediate states, the chain is still far from being fully collapsed and there is still, on average, a long distance between the two ends of the chain. Snapshots of such intermediate states, as the one shown in figure 10b, confirms the previous suggestion: between expanded open chains and the compact helicoidal states there exists a region of partially collapsed filaments in which a part of the filament is already in a compact state while the other parts are still in a expanded conformation, with the chain ends being separated by a relatively long distance. Those partially collapsed structures remember vaguely of the core-shell structures found in non-magnetic semiflexible attractive chains⁴³. Nonetheless in the present case, we have a core plus some loose tails rather than a shell surrounding a core. This behaviour comes from the anisotropic nature of the magnetic interactions which favour relative straight segments far from the core rather than the wrapping of the core by the non-collapsed part of the chain. It is not yet clear what the behaviour of the filament will be in the limit $N \rightarrow \infty$ when long non-collapsed segments may exist.

As we have shown above, the characterisation of this new transition from open expanded chains to partially collapsed states by using the specific heat is hard to be accomplished for $\eta < 0.20$. We found that the best observable to determine the transition point are the dR_g/dT curves (see bottom of figure 8). The maxima of the peaks of such function for $\eta = 0.15, 0.20$, coincide with the apparent position of the emerging peaks for the C_V at the highest temperature. It is worth to mention that this observable has been also success-

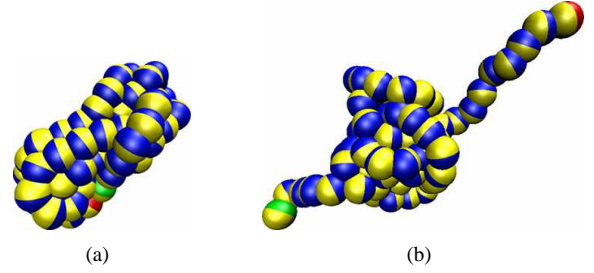


Fig. 10 The figure depicts two typical snapshots for high strengths of the LJ attractive interaction when compared to the strength of the magnetic interaction: (a) $\eta = 0.15$, $T = 0.40$. (b) $\eta = 0.20$, $T = 1.60$. The code of colours follows from figure 3.

fully used in the determination of conformational phase transitions of non-magnetic chains^{33,73}. Sharma and Kumar⁷⁸ have verified that the locations of peaks in structural and thermodynamic quantities accompanying conformational transitions of macromolecules do coincide in the limit of $N \rightarrow \infty$. For finite sizes, the two different types of observables may yield slightly different transition temperatures. However, in our case, the possible mismatches that could exist with respect the true transition temperature are below our accuracy in determining the transition points, and we do not expect such slight mismatches to substantially modify our sketch of the phase diagram for magnetic filaments. Results for the transition temperatures obtained via dR_g/dT are shown in figure 11 as solid blue triangles-up for all values of η .

3.3 The phase diagram for isolated flexible magnetic filaments

Gathering together the results presented in sections 3.1 and 3.2, it is possible to build up a tentative sketch of the (T, η) -phase diagram as shown in figure 11. The solid black circles correspond to the transition points for $\eta < 0.10$ derived from the position of the maxima of the peaks in the C_V and correspond to the transition from extended open chains to simple closed structures (see bottom plot in figure 4). Solid red squares depict the transition points obtained from the maximum of the highest peaks of the C_V in the range $T \in [0.7, 1.2]$, see figures 4 (top) and 8 (top). Those large peaks correspond to transitions towards a compact helicoidal state when the temperature is lowered. Solid green diamonds depict the transition points from compact helicoidal states to compact disordered states, which are obtained from the maxima of the peaks of the C_V in the region of very low temperatures $T < 0.7$ in figure 8 (top). The solid blue triangles-up correspond to the maxima of the peaks in the dR_g/dT , for $\eta \geq 0.1$, that also mark the inflection points of R_g , (figure 8, bottom). As we

described in section 3.2 the position of such peaks should basically coincide with the transition points from open extended chains to partially collapsed states. Figure 11 also shows that dR_g/dT does a very good estimation of the transition points from simple closed chains to helicoidal states, in which transition temperatures derived from dR_g/dT are very similar to those obtained from the position of the peaks in the C_V .

In figure 11 the solid black circles only refer to the transition for $\eta < 0.7$. This is due to the fact that, for higher values of η , the peak in the specific heat associated to such transition is hidden by the tail of the larger peak associated to the transition to helicoidal structures. In section 3.1 we mentioned the possibility of using the dR_{ee}/dT in order to characterise the transition from extended open chains to simple closed states. The inflection points of the $R_{ee}(T)$ curves are plotted in figure 11 as solid magenta down triangles. Furthermore, for values of $\eta < 0.1$ the inflection point in the end-to-end distance is clearly related to the transition point from open structures to simple closed structures. For values of $\eta \geq 0.1$ the inflection in the R_{ee} takes place approximately at the same temperature as the inflection point of R_g (solid blue triangles up) which, as discussed in section 3.1, is a consequence of the fact that a partial compaction of the chain triggers the closing of the chain.

A very remarkable fact observed in figure 11 is the existence of two different conformational 'triple points'. In the first 'triple point' extended open chains would coexist with partially collapsed states and simple closed states. In the second 'triple point', simple closed states will coexist with compact helicoidal states and partially collapsed states. The existence of two different, yet close triple points is a vivid example of how rich and complex the phase diagram for magnetic chains can be.

Finally, it is interesting to discuss how the phase diagram would change if the strength of the dipolar interaction μ^2 is modified, or if the range of the attractive forces is changed. To this end it is important to note that the bottom left corner of the phase diagram is dominated by the magnetic interactions, the upper left corner of the phase diagram is dominated by the LJ-like attractive interactions, and the bottom right corner is dominated by thermal motion. By increasing the dipolar strength μ^2 while keeping the other factors unaltered we should expect the region where the magnetic interactions are dominant to expand. That means that the transition from extended open chains to simple closed structures should shift towards higher temperatures, and the transition from simple closed structures to compact helicoidal states should occur at higher values of η . The region where partially collapsed structures exist should also shift towards regions of higher values of η and T . A reverse behaviour should be observed if we decrease the value of μ^2 rather than increasing it. On the other hand, if we increase the range of the attractive interactions, the region where

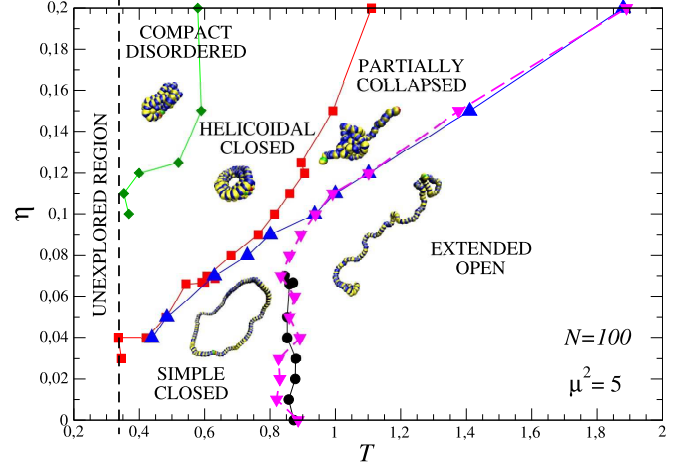


Fig. 11 A tentative phase diagram for magnetic filaments of length $N = 100$ and $\mu^2 = 5$ is presented. See text in section 3.3 for a detailed explanation of how the different transition lines were obtained. In sake of clarity of the origin of each transition line, they have been painted using different colours and symbols.

the attractive interactions dominate should expand, and therefore one should expect the transition from compact disordered structures to helicoidal states to occur at lower values of η . In turn, the transition from helicoidal to simple closed structures should also happen at lower values of η . It should be also possible to observe partially collapsed states at lower values of η .

4 Conclusions

A tentative phase diagram in the limit of infinite dilution for magnetic filaments made of $N = 100$ colloidal particles of identical size and magnetic momentum μ is presented as a function of the temperature and the relative strength between the attractive LJ-like interactions versus the dipolar magnetic moment, η . We have explored the range of parameters $T \in (0.27, 5)$ and $\eta \in [0, 0.2]$ via numerical simulations using Langevin dynamics. Our results evidence a rich phase diagram in which it has been possible to characterise up to five different conformational phases and two 'triple points'. In the first triple point, located in the nearby region to $(T \sim 0.9, \eta \sim 0.1)$, open chains, partially collapsed states and simple closed states will coexist, while in the second 'triple point', located in the nearby region to $(T \sim 0.6 - 0.8, \eta \sim 0.07 - 0.09)$, the three phases in coexistence are simple closed chains, compact helicoidal states, and partially collapsed states.

The characterisation of the different transition lines has been performed mainly via the analysis of the behaviour of the specific heat C_V , the radius of gyration R_g , and the end-to-

end distance R_{ee} . At low temperatures three different phases are found depending on the relative intensity of the attractive to the magnetic interaction: for low values of η simple chain-closed structures are observed, whereas for intermediate values of η compact helicoidal structures are developed. Both phases exhibit a considerable degree of anisotropy along the two major axis, where the structure is much more elongated along one of them. The helicoidal states become more isotropic as η increases. In the limit of strong attractive interactions (large η values), the helicoidal structure is lost and very compact disordered states with volumes close to the hexagonal-compact-package limit become the preferred states. Nonetheless, as figure 10a illustrates, the filaments do not develop, in the range of sampled temperatures, a crystal order.

Moreover at higher temperatures ($T \geq 1$) and low η the predominant states are extended open chains which exhibit a significant anisotropy due to the effects arising from the magnetic interactions that favour the formation of flat structures with long persistence lengths. In these structures, dipoles are aligned in a nose-tail orientation. Nonetheless, as temperature increases, in the limit $T \rightarrow \infty$, the structures are expected to become more isotropic and resemble a swollen self-avoiding random coil. By increasing η , a new kind of partially collapsed structure emerges. These structures are partially collapsed while keeping the two chain ends in a swollen conformation. The transition from extended open chains to partially collapsed states can be roughly characterised via the inflection points in the radius of gyration and the end-to-end distance. If the strength of the attractive interaction is further increased, a second transition from partially collapsed states to helicoidal states occurs. In this case, the transition can be monitored via the specific heat. This transition involves a severe rearrangement of the monomers and the peak associated to such transition can be easily identified. Though not observed in the range of η 's sampled, we speculate that at even higher strengths of the attractive interaction, a new transition from helicoidal state to compact disordered globules should occur.

Although the present phase diagram is only a simple sketch of a much more complex reality, interesting open questions emerge from it. One of them is, for instance, whether or not it is possible to find a critical η below which in the limit $T \rightarrow 0$ the only ground states are simple closed structures as those found for non-sticky filaments. The behaviour of the helicoidal states for $\eta \gg 0.2$ is another issue worth to be studied. As pointed out in section 3.1, helixes are energetically favoured over toroidal conformations for moderate values of η , but for increasing values of this parameter there is the possibility that helixes convert into toroidal structures quite similar to those observed in semi-flexible non-magnetic chains^{38,43}. It is yet unclear if compact helicoidal states will transit to compact globules directly, or rather they will do it via interme-

diate partially collapsed states where the existence of a third 'triple point' cannot be discarded. The structure of the ground states for the magnetic filaments, and up to which degree they show resemblances with the ground states observed for clusters of Stockmayer-particles⁶⁶, is also another open question. Finally, it will be also interesting to study how the phase diagram changes with the chain length N or with the polydispersity in size of the colloidal particles that form the magnetic filaments.

A good understanding of the different structures that magnetic filaments may adopt as a function of the interplay of the different interactions involved, and the phase diagram they display, is crucial in order to assess the use of these filaments for new technological applications or as substitutes of current ferrofluids with enhanced properties. Magnetic filaments have an enormous potential for new applications, and the characterisation of their properties is an open challenge. The present work represents a first step towards the understanding of the magnetic filaments that should stimulate further developments on this subject of increasing scientific interest.

Acknowledgements

Simulations were performed at the IFISC's Nuredduna high-throughput computing clusters, supported by the projects GRID-CSIC⁷⁹ and FISICOS (FIS2007-60327, funded by the Spanish MINCIN and the ERDF).

References

- 1 M. Kamachi, *J Macromol Sci-Pol R*, 2002, **C42**, 541–561.
- 2 S. J. Blundell and F. L. Pratt, *J Phys-Condens Mat*, 2004, **16**, R771–R828.
- 3 B. Y. Geng, J. Z. Ma, X. W. Liu, Q. B. Du, M. G. Kong and L. D. Zhang, *Appl Phys Lett*, 2007, **90**, 043120.
- 4 K. Ērglis, D. Zhulenkova, A. Sharipo and A. Cēbers, *J Phys-Condens Mat*, 2008, **20**, 204107.
- 5 H. Wang, Y. Yu, Y. Sun and Q. Chen, *Nano*, 2011, **06**, 1–17.
- 6 E. M. Furst, C. Suzuki, M. Fermigier and A. P. Gast, *Langmuir*, 1998, **14**, 7334–7336.
- 7 E. M. Furst and A. P. Gast, *Phys Rev Lett*, 1999, **82**, 4130–4133.
- 8 R. Dreyfus, J. Baudry, M. L. Roper, M. Fermigier, H. A. Stone and J. Bibette, *Nature*, 2005, **437**, 862–865.
- 9 O. Tabata, H. Kojima, T. Kasatani, Y. Isono and R. Yoshida, Proceedings IEEE Sixteenth Annual International Conference on Micro Electro Mechanical Systems, 2003, pp. 12–15.
- 10 H. Singh, P. E. Laibinis and T. A. Hatton, *Nano Lett*, 2005, **5**, 2149–2154.
- 11 H. Singh, P. E. Laibinis and T. A. Hatton, *Langmuir*, 2005, **21**, 11500–11509.
- 12 J. den Toonder, F. Bos, D. Broer, L. Filippini, M. Gillies, J. de Goede, T. Mol, M. Reijme, W. Talen, H. Wilderbeek, V. Khatavkar and P. Anderson, *Lab Chip*, 2008, **8**, 533–541.
- 13 F. Martínez-Pedrero, M. Tirado-Miranda, A. Schmitt and J. Callejas-Fernández, *Phys Rev E*, 2007, **76**, 011405.
- 14 F. Martínez-Pedrero, M. Tirado-Miranda, A. Schmitt and J. Callejas-Fernández, *J. Colloid. Int. Sci.*, 2008, **318**, 23–28.
- 15 Y. Liu and Q. Chen, *Nanotechnology*, 2008, **19**, 475603.

- 16 B. A. Evans, A. R. Shields, R. L. Carroll, S. Washburn, M. R. Falvo and R. Superfine, *Nano Lett*, 2007, **7**, 1428–1434.
- 17 Z. Zhou, G. Liu and D. Han, *ACS Nano*, 2009, **3**, 165–172.
- 18 P. Y. Keng, I. Shim, B. D. Korth, J. F. Douglas and J. Pyun, *ACS Nano*, 2007, **1**, 279–292.
- 19 S. E. Bowles, W. Wu, T. Kowalewski, M. C. Schalnatz, R. J. Davis, J. E. Pemberton, I. Shim, B. D. Korth and J. Pyun, *J Am Chem Soc*, 2007, **129**, 8694–8695.
- 20 J. J. Benkoski, S. E. Bowles, R. L. Jones, J. F. Douglas, J. Pyun and A. Karim, *J Polym Sci, Part B: Polym Phys*, 2008, **46**, 2267–2277.
- 21 J. J. Benkoski, S. E. Bowles, B. D. Korth, R. L. Jones, J. F. Douglas, A. Karim and J. Pyun, *J Am Chem Soc*, 2007, **129**, 6291–6297.
- 22 J. J. Benkoski, R. L. Jones, J. F. Douglas and A. Karim, *Langmuir*, 2007, **23**, 3530–3537.
- 23 J. J. Benkoski, H. Hu and A. Karim, *Macromol Rapid Commun*, 2006, **27**, 1212–1216.
- 24 J. J. Benkoski, R. M. Deacon, H. B. Land, L. M. Baird, J. L. Breidenich, R. Srinivasan, G. V. Clatterbaugh, P. Y. Keng and J. Pyun, *Soft Matter*, 2010, **6**, 602–609.
- 25 J. J. Benkoski, J. L. Breidenich, O. M. Uy, A. T. Hayes, R. M. Deacon, H. B. Land, J. M. Spicer, P. Y. Keng and J. Pyun, *J Mater Chem*, 2011, **21**, 7314–7325.
- 26 J. L. Breidenich, M. C. Wei, G. V. Clatterbaugh, J. J. Benkoski, P. Y. Keng and J. Pyun, *Soft Matter*, 2012, **8**, 5334–5341.
- 27 D. Sarkar and M. Mandal, *J. Phys. Chem. C*, 2012, **116**, 3227–3234.
- 28 C. Goubault, F. Leal-Calderon, J.-L. Viovy and J. Bibette, *Langmuir*, 2005, **21**, 3725–3729.
- 29 J. de Vicente, D. J. Klingenberg and R. Hidalgo-Alvarez, *Soft Matter*, 2011, **7**, 3701–3710.
- 30 J. Liu, Y. Mao and J. Ge, *Nanoscale*, 2012, **4**, 1598–1605.
- 31 Y. Zhou, M. Karplus, J. M. Wichert and C. K. Hall, *J Chem Phys*, 1997, **107**, 10691–10708.
- 32 T. Vogel, M. Bachmann and W. Janke, *Phys Rev E*, 2007, **76**, 061803.
- 33 D. T. Seaton, T. Wüst and D. P. Landau, *Phys Rev E*, 2010, **81**, 011802.
- 34 J. M. Polson, S. B. Opps and N. A. Risk, *J Chem Phys*, 2009, **130**, 244902.
- 35 S. Schnabel, T. Vogel, M. Bachmann and W. Janke, *Chem Phys Lett*, 2009, **476**, 201–204.
- 36 S. B. Opps, J. M. Polson and N. A. Risk, *J Chem Phys*, 2006, **125**, 194904.
- 37 J. M. Polson and N. E. Moore, *J Chem Phys*, 2005, **122**, 024905.
- 38 K. Binder, W. Paul, T. Strauch, F. Rampf, V. Ivanov and J. Luettmer-Strathmann, *Journal of Physics: Condensed Matter*, 2008, **20**, 494215.
- 39 B. M. Baysal and F. E. Karasz, *Macromol Theor Simul*, 2003, **12**, 627–646.
- 40 V. A. Ivanov, W. Paul and K. Binder, *J. Chem. Phys.*, 1998, **109**, 5659–na.
- 41 V. A. Ivanov, M. R. Stukan, V. V. Vasilevskaya, W. Paul and K. Binder, *Macromol Theor Simul*, 2000, **9**, 488–499.
- 42 M. R. Stukan, V. A. Ivanov, A. Y. Grosberg, W. Paul and K. Binder, *J Chem Phys*, 2003, **118**, 3392–3400.
- 43 Y. Higuchi, T. Sakaue and K. Yoshikawa, *Chem Phys Lett*, 2008, **461**, 42–46.
- 44 D. T. Seaton, S. Schnabel, M. Bachmann and D. P. Landau, *International Journal of Modern Physics C*, 2012, **23**, 1240004.
- 45 M. N. Bannerman, J. E. Magee and L. Lue, *Phys Rev E*, 2009, **80**, 021801.
- 46 S. A. Sabeur, F. Hamdache and F. Schmid, *Phys Rev E*, 2008, **77**, 020802.
- 47 T. Garel, H. Orland and E. Orlandini, *Eur Phys J B*, 1999, **12**, 261–268.
- 48 J.-H. Huang and M.-B. Luo, *Polymer*, 2004, **45**, 2863–2867.
- 49 M.-B. Luo, *J Chem Phys*, 2006, **124**, 034903.
- 50 M.-B. Luo and C. Qian, *Polymer*, 2006, **47**, 1451–1455.
- 51 J.-H. Huang, M.-B. Luo and C.-J. Qian, *J. Appl. Polym. Sci.*, 2006, **99**, 969–na.
- 52 C. Phatak, R. Pokharel, M. Beleggia and M. D. Graef, *J Magn Magn Mater*, 2011, **323**, 2912–2922.
- 53 K. I. Morozov and M. I. Shliomis, *Ferrofluids, Magnetically Controllable Fluids and Their Application*, Springer-Verlag, Heidelberg, 2002, pp. 162–184.
- 54 V. P. Shcherbakov and M. Winklhofer, *Phys. Rev. E*, 2004, **70**, 061803–na.
- 55 K. Ērglis, L. Alberte and A. Cēbers, *Magnetohydrodynamics*, 2008, **44**, 223–236.
- 56 S. L. Biswal and A. P. Gast, *Phys Rev E*, 2003, **68**, 021402.
- 57 A. Cēbers, *Curr Opin Colloid Interface Sci*, 2005, **10**, 167–175.
- 58 A. Cēbers and I. Javaitis, *Phys Rev E*, 2004, **69**, 021404.
- 59 M. Belovs and A. Cēbers, *Phys Rev E*, 2009, **79**, 051503.
- 60 M. Belovs, T. Čirulis and A. Cēbers, *J Phys A: Math Theor*, 2009, **42**, 235206.
- 61 A. Snezhko, M. Belkin, I. S. Aranson and W.-K. Kwok, *Phys. Rev. Lett.*, 2009, **102**, 118103.
- 62 F. Fahmi, M. W. J. Prins and L. J. van IJendoorn, *Lab Chip*, 2009, **9**, 3413–3421.
- 63 A. Babataheri, M. Roper, M. Fermigier and O. D. Roure, *Journal of Fluid Mechanics*, 2011, **678**, 5–13.
- 64 P. A. Sánchez, J. J. Cerdà, V. Ballenegger, T. Sintes, O. Piro and C. Holm, *Soft Matter*, 2011, **7**, 1809–1818.
- 65 P. A. Sánchez, J. J. Cerdà, T. Sintes and C. Holm, Submitted to the Journal of Chemical Physics.
- 66 M. A. Miller and D. J. Wales, *The Journal of Physical Chemistry B*, 2005, **109**, 23109–23112.
- 67 J. D. Weeks, D. Chandler and H. C. Andersen, *J Chem Phys*, 1971, **54**, 5237–5247.
- 68 M. P. Allen and D. J. Tildesley, *Computer Simulation of Liquids*, Clarendon Press, Oxford, 1st edn, 1987.
- 69 J. J. Cerdà, S. Kantorovich and C. Holm, *J Phys-Condens Mat*, 2008, **20**, 204125.
- 70 S. Kantorovich, J. J. Cerdà and C. Holm, *Phys Chem Chem Phys*, 2008, **10**, 1883–1895.
- 71 H. J. Limbach, A. Arnold, B. A. Mann and C. Holm, *Comput Phys Commun*, 2006, **174**, 704–727.
- 72 *Ferrofluids, Magnetically Controllable Fluids and Their Application*, ed. S. Odenbach, Springer-Verlag, Heidelberg, 2002.
- 73 D. F. Parsons and D. R. M. Williams, *Phys Rev E*, 2006, **74**, 041804.
- 74 D. Seaton, T. Wüst and D. Landau, *Computer Physics Communications*, 2009, **180**, 587–589.
- 75 T. Vogel, P. A. Sánchez, J. J. Cerdà, T. Sintes and C. Holm, In preparation.
- 76 T. A. Prokopenko, V. A. Danilov, S. S. Kantorovich and C. Holm, *Phys Rev E*, 2009, **80**, 031404.
- 77 J. P. Kemp and Z. Y. Chen, *Phys Rev Lett*, 1998, **81**, 3880–3883.
- 78 S. Sharma and S. K. Kumar, *J. Chem. Phys.*, 2008, **129**, 134901.
- 79 GRID-CSIC (<http://www.grid-csic.es>), Grid infrastructure for advanced research at the Spanish National Research Council, Ref. 200450E494.